The validity of plagioclase-melt geothermometry for degassing-driven magma crystallisation.

Humphreys, Madeleine C. S.[1], Edmonds, Marie[2] and Klöcking, Marthe S.[2]

[1] Department of Earth Sciences, Durham University, Science Labs, Durham, DH1 3LE, UK. Tel: +44 (0)191 334 2343. Email: madeleine.humphreys@durham.ac.uk

[2] Department of Earth Sciences, University of Cambridge, Downing Street, Cambridge, CB2 3EQ, UK

Abstract

Any quantitative interpretation of the formation conditions of igneous rocks requires methods for determining crystallisation temperature. Accurate application of such thermobarometers relies on the attainment of equilibrium in the system to be studied. This may be particularly difficult in silicic magmas, where diffusivities are low and crystallisation kinetics sluggish. Moreover, progressive degassing of volatile-rich magmas during ascent can result in continuous changes in effective undercooling, causing particular problems in achieving equilibrium between melt and crystals that grow in response to decompression. We consider these problems in the context of plagioclase-melt equilibria for magmas undergoing decompression and degassing-driven crystallisation, using two published thermometers. The two thermometers show similar trends with key parameters but absolute temperatures can vary by > 200 °C. Analysis of decompression experiments conducted at constant temperature shows systematic variations in calculated temperature and equilibrium constant with varying decompression rate and quench pressure. This indicates that

25 an unrecognised lack of equilibration could result in significant temperature
26 overestimates and potentially spurious results. This highlights the need to assess for
27 equilibrium, and we discuss problems associated with some commonly used
28 indicators of equilibration. Finally, retrospective analysis of published plagioclase-
29 hosted melt inclusion suites from five subduction zone volcanoes shows systematic
30 increases in calculated temperature and equilibrium constant with decreasing H_2O
31 concentration. While this could represent the signature of latent heat of
32 crystallisation, we suggest that such patterns should be treated with caution unless
33 there is clear evidence of sustained equilibrium between plagioclase and melt
34 during decompression.
35
36 **Introduction**
37 Thermometry and thermobarometry underpin igneous petrology as a quantitative
38 science. An ability to place quantitative estimates of temperature and pressure on
39 mineral ± melt assemblages observed in igneous rocks is fundamental to
40 understanding the conditions of magma storage, fractionation, ascent and eruption,
41 as well as melt generation processes, in any tectonic setting. For example,
42 clinopyroxene-melt thermobarometry was used to demonstrate that individual
43 eruptions in the Springerville volcanic field, Arizona, USA were derived from
44 different source regions in a vertically extensive mush reservoir, with magma
45 ponding levels influenced by changes in crustal rheology or density (Putirka and
46 Condit 2003). Cashman and Blundy (2013) used knowledge of plagioclase-melt
47 equilibria to reconstruct the pressure-temperature histories of individual,

48 complexly zoned plagioclase phenocrysts from Mount St Helens, USA. Hornblende
49 thermobarometry also appears to define vertically extensive crystallisation
50 conditions for magmas from Redoubt volcano (Alaska) and El Reventador
51 (Ecuador), amongst others (Ridolfi et al. 2010).

52 Although application of thermobarometry is now routine, it still has the
53 potential to prompt new interpretations about the ways that magmas evolve and
54 migrate. For example, Blundy et al. (2006) used the plagioclase-liquid thermometer
55 of Putirka (2005) to determine entrapment temperatures for suites of plagioclase-
56 hosted melt inclusions. The results showed strong increases in calculated
57 temperature with decreasing H_2O(m), interpreted as the result of latent heat release
58 during exothermic, decompression-driven crystallisation of silicic magmas. This is
59 significant because such release of latent heat could produce commonly observed
60 petrographic features, such as reversely zoned phenocryst rims, that might
61 otherwise be ascribed to late-stage mingling with hotter magma (Blundy et al.
62 2006). With the increasing availability of relatively large mineral and/or melt
63 datasets from electron microprobe and other analytical techniques, thermometers
64 are now routinely applied to whole datasets instead of carefully chosen individual
65 analyses. This has the potential to uncover subtle details that are only apparent at
66 the population level, but brings a risk of inadequate interrogation of equilibration
67 within the full dataset.

68 An important limitation is that in volcanic systems, where the timescales of
69 melt crystallisation, chemical diffusion or magma movement may be short,
70 geochemical equilibration between melt and mineral may be kinetically inhibited.

71 For example, both the major element composition and the trace element contents of
72 crystals are highly dependent on the degree of undercooling below the liquidus
73 temperature (e.g. Gamble and Taylor 1980; Kennedy et al. 1993; Dunbar et al. 1995;
74 Mollo et al. 2010, 2011b). Chemical diffusion rates can also be strongly dependent
75 on the concentrations of species that are involved in the reaction(s). This is not a
76 new problem and has been addressed by several authors historically, but is
77 particularly important in the context of degassing-driven processes in volatile-rich
78 magmas. In the context of thermobarometry, these factors represent varying
79 degrees of disequilibrium and have the potential to produce biased or spurious
80 temperatures if this is not recognised (e.g. Putirka 2008; Mollo et al. 2011b). In
81 particular, Mollo et al. (2010) and Mollo et al. (2011b) showed that increasing the
82 cooling rate of anhydrous basaltic melt from 0.5 to 15 °C/min could generate an
83 overestimate in calculated temperature of up to 150 °C.
84 Here, we highlight the problems of not recognising incomplete equilibration
85 in H_2O-bearing magmas, many of which crystallise due to decompression rather
86 than cooling (e.g. Geschwind and Rutherford 1995; Blundy and Cashman 2001),
87 where diffusivities are low and crystallisation kinetics may be very sluggish. In this
88 scenario, the *thermal* undercooling driving crystallisation may be negligible but
89 substantial effective undercoolings are still readily achieved by decompression and
90 water loss. We focus on plagioclase-melt thermometry and degassing-driven magma
91 crystallisation, which is particularly sensitive to the kinetics of crystal nucleation
92 and growth. Drawing on previously published natural datasets and experimental
93 studies, we demonstrate that disequilibrium crystallisation during degassing can

result in large errors in thermometry, and that this can lead to potentially very significant problems with obtaining a unique interpretation of the resultant P-T conditions.

Plagioclase-melt thermobarometry

Plagioclase-melt thermometers are based on equilibrium exchange of albite and anorthite components between solid (s) and melt (m):

$$An_{(m)} + Ab_{(s)} = An_{(s)} + Ab_{(m)} \quad [1]$$

with the equilibrium constant expressed as (Putirka 2005; Putirka 2008):

$$K_D = (X_{An}^{pl} * Ca^{L} * Al^{L}) / (X_{Ab}^{pl} * Na^{L} * Si^{L}) \quad [2]$$

where (e.g.) Ca^{L} refers to the anhydrous cation fraction of Ca in the liquid. The composition of plagioclase crystallising from a melt is controlled by temperature, melt composition and melt H_2O concentration. In anhydrous melts, the equilibrium plagioclase composition shifts systematically towards albite with decreasing temperature (e.g. (Bowen 1913; Kudo and Weill 1970; Drake 1976). In hydrous melts, the shape of the albite-anorthite binary loop in T-X space is broadened and shifted to lower temperature relative to anhydrous compositions (Kudo and Weill 1970; Drake 1976; Johannes 1984). This may be because OH tends to complex with Na and SiO_4 groups in preference to Ca and AlO_4, particularly at higher temperature (Lange et al. 2009). This means that addition of H_2O causes a decrease in activity of the albite component of the melt, aAb(m), relative to aAn(m) and the liquidus plagioclase composition therefore becomes more calcic (e.g. Arculus and Wills 1980; Housh and Luhr 1991; Sisson and Grove 1993; Panjasawatwong et al. 1995).

We focus on two of the most recently published plagioclase-melt thermometers: model A of Putirka (2005) and the plagioclase-melt hygrometer of Lange et al. (2009). The latter has been recalibrated and updated by Waters and Lange (in press). Both models are based on empirical regression of thermodynamically derived expressions. Calibration of both models was done using large databases of phase equilibrium experiments that crystallised plagioclase over a range of pressures, temperatures and H_2O concentrations. A second set of experiments was used to test each model. The Putirka model (model A) was calibrated on basaltic to rhyolitic liquids that crystallised plagioclase from 0.001-13 kbar, 998-1623 K and H_2O concentrations up to 15 wt%. According to the test data, the model returns temperature with a standard error estimate of ± 23 K (Putirka 2005). A later independent test using a larger dataset of additional experiments gave an average absolute deviation of ±19 °C and propagated uncertainty of ± 7 MPa for experiments on hydrous rhyolite at 750-995 °C and 15-313 MPa (Blundy et al. 2006). The Lange et al. (2009) hygrometer was calibrated on rhyolitic melts with <30 vol% crystals at 925-1100 °C, 48-300 MPa and 2.2-7.0 wt% H_2O. Temperatures were recovered for the test data with an average uncertainty of ± 14 °C, while the standard error estimate for H_2O was ± 0.32 wt% (Lange et al. 2009).

Comparison of the thermobarometers

We first used each of the two thermometers to predict the shape of constant-X_{An} contours in H_2O-T space (figure 1) for a representative rhyolitic matrix glass

140 composition from Soufrière Hills volcano, Montserrat (table 1), for comparison with
141 the experimental study of Couch et al. (2003). For the Lange thermometer, this
142 involved supplying X_{An}, T, P and melt composition to the model and retrieving melt
143 H_2O over a range of temperatures. We ran these calculations using pressures of 10
144 MPa and 200 MPa, but this made little difference to the absolute H_2O concentrations
145 retrieved and had no effect on the shape of the X_{An} contours. We therefore
146 subsequently assumed H_2O-saturated conditions and calculated $P_{tot} = pH_2O$ using
147 VolatileCalc (Newman and Lowenstern 2002) (we define pH_2O as the partial
148 pressure of H_2O, which for a pure H_2O magmatic component is the total confining
149 pressure at volatile saturation for a given H_2O concentration). For the Putirka
150 thermometer we supplied X_{An}, H_2O content, P and melt composition and retrieved
151 temperature, again assuming that $P_{tot} = pH_2O$.
152
153 Both models calculate an increase in temperature with decreasing H_2O
154 concentration at constant X_{An} and fixed melt composition (figure 1a), as expected.
155 Equivalent calculations using a basaltic-andesite melt from Hamada & Fujii (2007;
156 see table 1) produce parallel curves offset to higher temperature at the same H_2O
157 concentration. However, the overall results are highly model-dependent,
158 particularly at low H_2O concentrations where there are big disparities between
159 temperatures predicted for a given X_{An}. For example, at 20 MPa (1.3 wt% H_2O,
160 volatile-saturated) plagioclase of composition An_{70} is predicted to occur in H_2O-
161 saturated melt at 951 °C using Putirka (2005) but at >1300 °C using Lange et al.
162 (2009) (figure 1a). This indicates that application of plagioclase-melt equilibria to

give *absolute* temperature estimates must be subject to at least some uncertainty. Data from the phase equilibrium experiments of Couch et al. (2003), which were used as a calibration dataset for Lange et al. (2009) but not for Putirka (2005), lie between the two models (figure 1a).

Figure 1

Secondly, we calculated temperature contours in H_2O – X_{An} space, which show a positive correlation of X_{An} with H_2O concentration at constant temperature (figure 1b). The results are similarly model-dependent, with only minor variations in slope of the temperature contours but significant variations in the absolute H_2O concentration predicted to be in equilibrium with a given plagioclase composition. In comparison, RhyoliteMELTS (Gualda et al. 2012) isothermal decompression runs and the data from Couch et al. (2003) show a much steeper variation of X_{An} with H_2O (figure 1b).

Figure 2

Finally, we calculated isobaric contours for H_2O-saturated rhyolite in T-X_{An} space; these define a positive correlation of temperature with X_{An} (figure 2). The two models agree well at lower temperature and more sodic plagioclase compositions but diverge with increasing temperature and X_{An}. RhyoliteMELTS isobaric cooling runs are offset towards lower temperature and lower X_{An}, and with steeper slope in

186 T-X_{An} space, than either of the other two thermobarometers (figure 2). The data
187 from Couch et al. (2003) are offset to higher X_{An} relative to the Lange model and
188 have a steeper slope than the Putirka model (figure 2).
189
190 *Figure 3*
191
192 As a possible test for equilibrium in the system $Ca_2Al_2Si_2O_8$ – $NaAlSi_3O_8$ – H_2O –
193 silicate melt, the albite-anorthite distribution coefficient, K_D (equation [2]) is
194 reported to be normally distributed with values of 0.10 ± 0.05 for T < 1050 °C
195 (mostly hydrous) and 0.27 ± 0.11 for T ≥ 1050 °C (Putirka 2008). To assess the
196 significance of individual external parameters in contributing to this variation, we
197 retrieved K_D from the equilibrium calculations described above, using the Putirka
198 thermometer. Importantly, the results show that for a fixed melt composition and
199 fixed H_2O concentration *at equilibrium conditions*, variations in X_{An} cause K_D to
200 decrease systematically with increasing temperature (figure 3a). Similarly, for a
201 fixed melt composition at equilibrium at a constant calculated temperature, the link
202 between X_{An} and pH_2O means that K_D decreases systematically with increasing X_{An}
203 or increasing pH_2O (figure 3b,c). These variations mean that the equilibrium
204 constant cannot easily be used to assess whether equilibrium has been achieved.
205
206 **pH_2O – T profiles of decompression experiments**
207 Both thermobarometers were originally calibrated and tested using phase
208 equilibrium studies at fixed P, T conditions. However, many of their potential

applications are for magmas that have experienced more dynamic conditions, including degassing-induced crystallisation. To test the applicability of the thermobarometers for these conditions in natural volatile-rich magmas, we used the results of three sets of decompression experiments that crystallised plagioclase from hydrous, silicic melt at variable decompression rates representative of typical intermediate magma ascent. Cichy et al. (2011) performed isothermal decompression experiments on a synthetic, H_2O-bearing Unzen rhyodacite melt composition at 850 °C and at decompression rates from 0.0002 to 20 MPa/s. Glass H_2O contents were analysed by FTIR but represent incomplete (disequilibrium) degassing due to retarded bubble nucleation (Cichy et al. 2011). Secondly, Martel and Schmidt (2003) ran both isobaric and decompression experiments on H_2O-saturated, synthetic rhyolitic melt at 860 °C and 15-170 MPa, at decompression rates from 0.000017 – 16 MPa/s. Thirdly, Brugger and Hammer (2010) performed two series of experiments using used a crushed natural rhyodacitic starting material: one set of experiments was quenched along a decompression path ('snapshots') and the other set was allowed to anneal at the final pressure. Decompression rates varied between 0.008 and 0.17 MPa/s. For each experimental dataset, we took the glass composition, H_2O concentration of the glass (either calculated as volatiles by difference or from published measurements, see supplementary data table) and coexisting plagioclase composition to calculate the equilibrium temperature (T_{calc}, see supplementary data table). Except for mixed volatile (H_2O+CO_2) experiments we assumed melt H_2O saturation, and used VolatileCalc (Newman and Lowenstern 2002) to convert H_2O concentration to pH_2O

232 in MPa. This is important because in all three experimental studies, H_2O degassing
233 was retarded relative to equilibrium, showing higher concentrations in the glass
234 than the solubility at the experimental quench pressure (figure 4). Treating the data
235 in this way as volatile-saturated 'unknowns' therefore results in anomalously high
236 estimates of P_{tot}.
237
238 *Figure 4*
239
240 Application of the Putirka thermometer to data from the Martel and Schmidt
241 (2003) and Brugger and Hammer (2010) experimental series shows a general
242 pattern of increasing T_{calc} and decreasing K_D with decreasing pH_2O (figure 5), even
243 though the experiments were run at controlled temperature. Temperatures
244 calculated from the 'low pressure' experiments of Martel and Schmidt (2003) are
245 scattered within ± 45 °C of the experimental run temperature (860 ± 5 °C, Martel
246 and Schmidt 2003), whereas the 'high pressure' experiments are systematically
247 offset to significantly higher calculated temperatures, up to 84 °C greater than the
248 experimental run temperature (figure 5). Their isobaric experiments also show an
249 increase of T_{calc} with decreasing pH_2O (see supplementary data table). In contrast,
250 temperatures for data from the Brugger and Hammer (2010) experiments are
251 typically lower than the experimental run temperature (figure 5). The glass
252 compositions in all experiments show clear trends of increasing K_2O and decreasing
253 CaO content as pH_2O decreases due to progressive decompression, degassing and
254 crystallisation (see supplementary data table). The annealed experiments from

255 Brugger and Hammer (2010) had a more Al-poor, K-rich and Si-rich residual melt
256 composition and crystallised more albitic plagioclase; consequently temperatures
257 calculated from these data are slightly lower at a given pH_2O than the snapshot
258 experiments.
259
260 *Figure 5*
261
262 Temperatures calculated from Martel and Schmidt (2003) generally show an
263 increase with increasing decompression rate except at the very highest
264 decompression rates (>10 MPa/s); calculated K_Ds increase systematically with
265 increasing decompression rate (figure 6) and with T_{calc} (supplementary data table).
266 In contrast, the Brugger & Hammer data show no variation of either T_{calc} or K_D with
267 decompression rate (figure 7), and no variation of K_D with T_{calc}, over the more
268 limited range of decompression rates (see supplementary data table).
269
270 *Figure 6*
271
272 Fewer data are available for the Cichy et al. (2011) experiments but the available
273 data give higher (and more scattered) calculated temperatures and lower K_D at
274 lower pH_2O (figure 5). In contrast, there are clear increases in both T_{calc} and K_D with
275 increasing decompression rate, similar to calculations from the experiments of
276 Martel & Schmidt (figure 6), and K_D increases systematically with T_{calc} (see

277 supplementary data table). The glass compositions also change systematically as a
278 function of both pH_2O and decompression rate (supplementary data table).
279
280 The same patterns of T_{calc} are also seen using the Lange et al. (2009)
281 thermometer. The two sets of calculated temperatures correlate reasonably well but
282 those calculated using Lange et al. (2009) are typically significantly higher.
283 Meaningful temperatures commonly cannot be returned for evolved melts with low
284 H_2O content. This is due to an instability in the calculation of aAb(m) for
285 temperatures ≥1200 °C, which has been corrected by the recalibrated version of the
286 hygrometer (Waters and Lange in press; Lange & Waters, personal communication).
287 For this reason, and because the same trends were observed with both models, we
288 only used the Putirka thermometer for subsequent analysis of natural datasets (see
289 below).
290

291 **pH_2O-T profiles of magmas recorded in melt inclusions**

292 We applied a similar approach to populations of plagioclase-hosted melt inclusions
293 where the composition of coexisting melt and feldspar and the H_2O content of the
294 melt are both known, following Blundy et al. (2006). This allowed us to calculate the
295 apparent equilibrium temperature of entrapment for each melt inclusion and
296 plagioclase host pair, resulting in arrays of pH_2O-T coordinates (see supplementary
297 data table) and thus apparent magma ascent paths in pH_2O-T space. We examined
298 suites of melt inclusion data from the literature for Mount St Helens, USA (Blundy et
299 al. 2006); Shiveluch Volcano, Kamchatka (Blundy et al. 2006); Soufrière Hills,

Montserrat (Humphreys et al. 2009a, 2010); Unzen, Japan (Botcharnikov et al. 2008) and Izu-Oshima, Japan (Hamada and Fujii 2007). All datasets show a clear increase in T_{calc} with decreasing melt H_2O (figure 7), approximately parallel to constant-X_{An} contours shown in figure 1, as previously reported for Mount St Helens and Shiveluch by Blundy et al. (2006). There is only a slight positive correlation of T_{calc} with X_{An} for the dataset as a whole (figure 7). For the rhyolitic melts (Soufrière Hills, Mount St Helens and Shiveluch), calculated K_Ds are low and typically decrease systematically with increasing X_{An} in the host plagioclase and increase systematically with increasing melt H_2O concentration (figure 8); the latter is the opposite to the trend observed for the equilibrium calculations (see figure 3). Calculated K_Ds are higher for the andesitic (Unzen) and basaltic andesite (Izu Oshima) melts but the same trends are observed (figure 8).

Figure 8

Regression of T_{calc} for each dataset with the individual parameters that contribute to the temperature calculation typically gives $R^2 \leq 0.92$ for correlation of T_{calc} with H_2O and low to insignificant R_2 (typically ≤ 0.25) for other parameters (figures 9, 10). This indicates that up to 92% of the total variability in T_{calc} from each case study results from variability in melt H_2O concentrations, typically with little effect of changing melt or plagioclase composition. This is reinforced by the fact that 'ruptured' melt inclusions (those known from their major element composition to have leaked H_2O, (Blundy and Cashman 2005; Blundy et al. 2008) give anomalously

high calculated temperatures, some in excess of 1000 °C (figure 7; supplementary data table). In fact, the full range of T_{calc} recorded by each dataset can be reproduced by manually changing the H_2O concentration of any individual inclusion, whereas the host plagioclase composition has relatively little effect on T_{calc}.

Figures 9, 10

Discussion

Degassing-induced crystallisation under disequilibrium conditions?

Our analysis shows that many arc magmas (all those examined) show evidence of apparent heating during degassing-induced crystallisation driven by decompression. Decreasing melt H_2O concentration is the primary factor that drives the increase in calculated temperature, accounting for up to 92% of the observed variations in T_{calc}. Experimental studies where volatile-saturated melt is decompressed at constant temperature also show the same effect, giving systematic increases in T_{calc} with decreasing melt H_2O concentration. Studies that covered a wide range of decompression rates also show a systematic increase of T_{calc} with increasing decompression rate, although the Brugger & Hammer dataset shows that absolute temperature may not always be overestimated (see below). Finally, the equilibrium constant for reaction of plagioclase and melt also varies systematically with both melt H_2O concentration and decompression rate. These observations suggest that the calculated temperatures in the systems examined may reflect a disequilibrium process of volatile degassing and melt crystallisation. This arises

346 because crystal nucleation and growth at low pH_2O is hindered by the increasing
347 diffusivities of components within the melt, which are intimately linked to
348 degassing kinetics and temperature (e.g. Cashman and Blundy 2000; Hammer and
349 Rutherford 2002; Couch et al. 2003b; Brugger and Hammer 2010). A lack of
350 equilibrium in the decompression experiments is evidenced by variations in crystal
351 size distribution and degree of plagioclase saturation, and progressive changes
352 towards disequilibrium crystal morphologies with increasing decompression rate
353 (Brugger and Hammer 2010). The slow equilibration process is also indicated by
354 the slightly lower calculated temperatures retrieved (see figure 5) and more Ab-
355 rich plagioclase crystallised in their series of experiments that were annealed at
356 constant temperature following decompression, and by the failure of the MELTS
357 algorithm to predict melt compositions for experiments quenched at <45 MPa
358 (Brugger and Hammer 2010). Finally, the systematic variations of K_D with
359 temperature, pH_2O and decompression rate in the experimental studies clearly
360 show that these do not represent equilibrium conditions.

361 All the experimental studies examined here report a range of plagioclase
362 compositions for each run. Plagioclase compositions closest to equilibrium are
363 typically found at the crystal rim, with early-formed, more calcic plagioclase
364 preserved in the cores (Martel and Schmidt 2003; Brugger and Hammer 2010;
365 Waters 2013). This is explained by crystallisation during increasing extents of
366 effective undercooling, ΔT_{eff} (defined as $T_{liquidus} - T_{magma}$, see Crabtree and Lange
367 2011). Initially, crystallisation is inhibited relative to the equilibrium case, resulting
368 in lower volumes of plagioclase growth; insufficient time available for complete re-

equilibration means that as melt H_2O continues to change, new growth is added as more Ab-rich plagioclase, closer to equilibrium compositions (Brugger and Hammer 2010).

How accurate are calculated temperatures?

Perhaps most significantly, there is poor agreement between the two thermometers examined here, except for H_2O-rich melts and more albitic plagioclase (see figures 1 and 2). This means that it is difficult to be confident about the significance of absolute calculated temperatures, although relative variations appear robust. Secondly, crystallisation temperatures can be significantly over-estimated in the system plagioclase-melt-H_2O if disequilibrium is not recognised. This is consistent with observations of (Mollo et al. 2010, 2011) for both plagioclase and clinopyroxene in anhydrous basalt. Such disequilibrium would most likely take the form of hindered H_2O degassing into vesicles, disequilibrium crystallisation of anomalously An-rich plagioclase, or (for melt inclusions) variable loss of H from the inclusions after entrapment (see later). Our analysis shows that increases in T_{calc} can reflect increasing ΔT_{eff} due to changes in melt H_2O during decompression, as the melt viscosity increases and the kinetics of crystallisation become sluggish, rather than real increases in magma temperature. This means that, without an independent measure of ΔT_{eff}, it is difficult to interpret significant increases in calculated temperature during magma ascent as unequivocally due to latent heat of crystallisation (Blundy et al. 2006).

392 However, substantial release of latent heat is predicted on theoretical grounds, as
393 the primary driving force for crystallisation during decompression of volatile-
394 saturated magma is H_2O loss from the melt (Blundy et al. 2006). Thermodynamic
395 calculations indicate that plagioclase crystallisation from an anhydrous melt would
396 result in temperature increase of ~2.3 °C per 1% crystallisation (Couch et al. 2001),
397 while the assemblage plagioclase + orthopyroxene + oxides would give ~3.2 °C per
398 1% (Blundy et al. 2006). For the natural datasets studied here, the temperatures
399 estimated from plagioclase-liquid thermometry are typically well matched by two-
400 oxide temperatures, including for Mount St Helens and Shiveluch (Blundy et al.
401 2006) and Soufrière Hills, Montserrat (two-oxide microphenocryst or microlite
402 temperatures 958-1017 °C, Humphreys et al. 2009b; temperatures up to ~968 °C
403 from plagioclase-liquid thermometry, this study). For Unzen, oxide equilibria
404 indicate that the pre-eruptive magma was stored at ~790 °C whereas groundmass
405 oxides give temperatures of ~890 °C (Venezky & Rutherford 1999), and
406 plagioclase-liquid temperatures are significantly higher (900–1080 °C, see figure
407 10). However, we note that even though in some cases plagioclase-liquid
408 temperatures calculated from Putirka (2005) and 2-oxide temperatures are very
409 similar, the available two-oxide temperatures would not be in agreement with any
410 of the plagioclase-liquid temperatures calculated using the Lange et al. (2009)
411 model. Variably high 2-oxide temperatures may otherwise be ascribed to magma
412 mixing immediately prior to eruption (e.g. Devine et al. 2003; Blundy et al. 2006).
413

414 We are not aware of any further temperature estimates for Izu Oshima volcano, but
415 Hamada and Fujii (2007) interpreted the variations in H_2O concentration in their
416 melt inclusion suite as the result of variable H_2O loss from the inclusions. A similar
417 interpretation has been proposed to explain the variable H_2O contents of
418 plagioclase-hosted melt inclusions from Soufriere Hills Volcano, as a result of rapid
419 diffusional re-equilibration of H_2O through the phenocryst host (Mann et al. 2013).
420 If this were the case, then the significant increase in calculated temperature seen in
421 both datasets would result from disequilibrium driven by diffusive H loss from the
422 inclusions, with the inclusion and host unable to re-equilibrate except on much
423 longer timescales. This is also equivalent to the 'ruptured' melt inclusions from
424 Mount St Helens (Blundy et al. 2008), which are known to have undergone
425 syneruptive leakage of H_2O and which give anomalously high calculated
426 temperatures (see figure 7).
427
428 Although overall the experimental data show similar patterns of calculated
429 temperature, there are clear differences between studies. The experiments of
430 Martel and Schmidt (2003) and Cichy et al. (2011) give calculated temperatures
431 that are mostly too high, and are consistent with experimental run conditions only
432 at high pH_2O (figure 5c, e) and for the 'low pressure' series of Martel & Schmidt
433 (2003). However, the Brugger and Hammer (2010) dataset consistently
434 underestimates the known experimental run conditions, even though the same
435 pattern of increasing temperature with decreasing pH_2O is still observed (figure
436 5a). A potentially significant difference between these studies is that Brugger and

437 Hammer (2010) used a crushed natural starting material while both Martel and
438 Schmidt (2003) and Cichy et al. (2011) used synthetic starting materials made from
439 mixed powders. The use of different starting materials could affect the degree of
440 approach to equilibrium during the experiments, particularly for experiments that
441 cover a broad range of P-T-H_2O conditions (Pichavant et al. 2007).
442
443 An important final question is how to assess the accuracy of calculated
444 temperatures, or ΔT_{eff}, in natural magmas. For the experiments, accuracy is simple
445 to gauge by comparison with the known experimental temperature. However, for
446 natural melt inclusion datasets (or crystal rim – host melt pairs) this is impossible
447 without an independent measure of temperature and/or ΔT_{eff}. Any calculated
448 temperature using the plagioclase-liquid thermometer should therefore be
449 considered as a maximum unless there is clear evidence of equilibrium (see below).
450 Ideally, ΔT_{eff} should be constrained independently, but in practice this is difficult.
451 Integration of quantitative or qualitative textural studies with minor or trace
452 element partitioning, which is known to be strongly dependent on ΔT (e.g. Gamble
453 and Taylor 1980), may represent one path towards obtaining a less equivocal
454 measure of the degree of disequilibrium in natural systems. However, we suggest
455 that calculated K_D that are within the 'equilibrium range' of 0.10 ± 0.05 (for
456 temperatures < 1050 °C, Putirka 2008) are not sufficient to indicate complete
457 equilibration. Even the isobaric experiments of Martel and Schmidt (2003) show a
458 small but systematic decrease in K_D from 0.06 to 0.03 for a pressure range of 170 to

459 50 MPa, and this also reflects our calculations at fixed pH_2O and melt composition
460 (see figure 3; supplememtary data table).
461
462 **Broader constraints on determining equilibrium in melt inclusions**
463 It is commonly assumed that melt inclusion glass is in equilibrium with the host
464 mineral, based on observing whether the inclusions have euhedral 'negative crystal'
465 shapes or are rounded. The faceted negative crystal shapes are typically interpreted
466 as equilibrated, but in fact the texturally equilibrated shape moves towards rounded
467 surfaces with constant mean curvature in an attempt to minimise interfacial energy
468 (e.g. Bulau et al. 1979). Chemically, equilibrium in melt inclusions is commonly
469 tested by calculating the apparent mineral-melt K_D for the inclusion and its host
470 phenocryst, as described above for plagioclase-hosted melt inclusions. For slowly
471 equilibrating crystals, complex zoning textures in the host phase around the
472 inclusion may be clearly obvious using light microscopy or scanning electron
473 microscopy. However, in more rapidly equilibrating systems (e.g. olivine-hosted
474 inclusions) the major element Mg-Fe profiles may appear equilibrated while
475 significant chemical zoning of minor or trace components (e.g. Cr, Ni, P, Al) may still
476 be present, either within the host grain (e.g. Milman-Barris et al. 2008) or at the
477 margins of the melt inclusions (Newcombe et al. 2014). This is demonstrated by P
478 mapping of slowly cooled cumulate olivines that retained compositional zoning
479 features from a primary dendritic crystal architecture (Welsch et al. 2014).
480 Depending on whether the thermometer of choice involves major elements or trace
481 components, these issues may be significant or unimportant.

Figure 11

For plagioclase, diffusivities are overall much lower than in olivine, so major element zonation is usually clearly evident (figure 11). Melt inclusions in plagioclase commonly appear to be linked to periods of partial dissolution of the crystal, suggesting that formation of a rough interface predisposes the crystals towards melt entrapment. In some cases, it may be possible to deduce the most likely 'equilibrium' host plagioclase from careful examination of the plagioclase zoning textures (figure 11; Blundy and Cashman 2005; Humphreys et al. 2008). In other cases, petrographic examination shows that melt inclusions form an irregular, interconnected network in 3D, linked to either significant partial dissolution of the crystal during its evolution (reaction-controlled entrapment), or skeletal or hopper growth forms (growth entrapment). It may be very difficult to distinguish these two processes, particularly in crystals where partial textural equilibration has occurred leading to rounding of primary skeletal facets. Similar textures to those observed in plagioclase are also seen in both hornblende-hosted and pyroxene-hosted melt inclusions, and we suggest that further careful X-ray mapping in olivine is likely to show that these same processes are also present in olivine-hosted melt inclusions.

Implications

An analysis of variations in temperature calculated using two published plagioclase-liquid thermometers shows that disequilibrium conditions can result in significant

505 temperature overestimates for the system melt-plagioclase-H_2O. Differences in
506 temperature calculated by the different models imply that *absolute* temperatures
507 returned by the models should not be used with too much certainty. Systematic
508 variations in both calculated temperature and K_D are observed with increasing
509 decompression rate in isothermal decompression experiments. This implies that
510 disequilibrium degassing of H_2O from the melt is an important control on calculated
511 temperatures, and/or that growth of the equilibrium feldspar composition becomes
512 impeded during H_2O degassing as melt viscosity and species diffusivities increase.
513 Several natural melt inclusions datasets were examined and each shows a clear
514 trend of apparent heating with decreasing melt H_2O content. This could imply that
515 significant latent heating during degassing-induced crystallisation is a generic
516 feature of subduction zone volcanoes, or that syn-eruptive or post-entrapment H_2O
517 loss from melt inclusions during disequilibrium crystallisation is a significant
518 process in degassing magmas. We suggest that the calculated temperatures should
519 be treated as maxima unless there is direct evidence of equilibrium between
520 plagioclase and melt.
521

522 **Acknowledgements**

523 MCSH acknowledges support from a Royal Society University Research Fellowship.
524 We are grateful to Caroline Martel for provision of unpublished glass compositional
525 data and to Becky Lange and Laura Waters for discussion and advance access to
526 their recalibrated hygrometer. We acknowledge useful discussions with Jon Blundy,

527 Kathy Cashman, Keith Putirka, Tom Sisson and Julia Hammer, and journal reviews
528 from Fidel Costa and an anonymous reviewer.

529

530 **References**

531 Arculus, R.J., and Wills, K.J.A. (1980) The petrology of plutonic blocks and inclusions
532 from the Lesser Antilles Island Arc. Journal of Petrology, 21, 743–799.

533 Blundy, J., and Cashman, K. (2001) Ascent-driven crystallisation of dacite magmas at
534 Mount St Helens, 1980–1986. Contributions to Mineralogy and Petrology, 140,
535 631–650.

536 ——— (2005) Rapid decompression-driven crystallization recorded by melt inclusions
537 from Mount St. Helens volcano. Geology, 33, 793–796.

538 Blundy, J., Cashman, K., and Humphreys, M. (2006) Magma heating by decompression-
539 driven crystallization beneath andesite volcanoes. Nature, 443, 76–80.

540 Blundy, J., Cashman, K.V., and Berlo, K. (2008) Evolving magma storage conditions
541 beneath Mount St. Helens inferred from chemical variations in melt inclusions
542 from the 1980-1986 and current (2004-2005) eruptions. In A volcano rekindled:
543 The renewed eruption of Mount St. Helens, 2004-2006 Vol. 1750, pp. 755–790.

544 Botcharnikov, R.E., Holtz, F., Almeev, R.R., Sato, H., and Behrens, H. (2008) Storage
545 conditions and evolution of andesitic magma prior to the 1991–95 eruption of
546 Unzen volcano: Constraints from natural samples and phase equilibria
547 experiments. Journal of Volcanology and Geothermal Research, 175, 168–180.

548 Bowen, N.L. (1913) The melting phenomena of the plagioclase feldspar. American
549 Journal of Science, 35, 577–599.

550 Brugger, C.R., and Hammer, J.E. (2010) Crystallization Kinetics in Continuous
551 Decompression Experiments: Implications for Interpreting Natural Magma Ascent
552 Processes. Journal of Petrology, 51, 1941–1965.

553 Bulau, J.R., Waff, H.S., and Tyburczy, J.A. (1979) Mechanical and thermodynamic
554 constraints on fluid distribution in partial melts. Journal of Geophysical Research,
555 84, 6102–6108.

556 Cashman, K., and Blundy, J. (2000) Degassing and crystallization of ascending andesite
557 and dacite. Philosophical Transactions of the Royal Society of London. Series A:
558 Mathematical, Physical and Engineering Sciences, 358, 1487–1513.

——— (2013) Petrological cannibalism: the chemical and textural consequences of incremental magma body growth. Contributions to Mineralogy and Petrology, 166, 703–729.

Cichy, S.B., Botcharnikov, R.E., Holtz, F., and Behrens, H. (2011) Vesiculation and Microlite Crystallization Induced by Decompression: a Case Study of the 1991-1995 Mt Unzen Eruption (Japan). Journal of Petrology, 52, 1469–1492.

Couch, S., Sparks, R.S.J., and Carroll, M.R. (2001) Mineral disequilibrium in lavas explained by convective self-mixing in open magma chambers. Nature, 411, 1037–1039.

Couch, S., Harford, C.L., Sparks, R.S.J., and Carroll, M.R. (2003a) Experimental constraints on the conditions of formation of highly calcic plagioclase microlites at the Soufrière Hills Volcano, Montserrat. Journal of Petrology, 44, 1455–1475.

Couch, S., Sparks, R.S.J., and Carroll, M.R. (2003b) The kinetics of degassing-induced crystallization at Soufriere Hills Volcano, Montserrat. Journal of Petrology, 44, 1477–1502.

Crabtree, S.M., and Lange, R.A. (2011) Complex Phenocryst Textures and Zoning Patterns in Andesites and Dacites: Evidence of Degassing-Induced Rapid Crystallization? Journal of Petrology, 52, 3–38.

Devine, J.D., Rutherford, M.J., Norton, G.E., and Young, S.R. (2003) Magma storage region processes inferred from geochemistry of Fe-Ti oxides in andesitic magma, Soufriere Hills Volcano, Montserrat, W.I. Journal of Petrology, 44, 1375–1400.

Drake, M.J. (1976) Plagioclase-melt equilibria. Geochimica et Cosmochimica Acta, 40, 457–465.

Dunbar, N.W., Jacobs, G.K., and Naney, M.T. (1995) Crystallization processes in an artificial magma: variations in crystal shape, growth rate and composition with melt cooling history. Contributions to Mineralogy and Petrology, 120, 412–425.

Gamble, R.P., and Taylor, L.A. (1980) Crystal/ liquid partitioning in augite: Effects of cooling rate. Earth and Planetary Science Letters, 47, 21–33.

Geschwind, C.-H., and Rutherford, M.J. (1995) Crystallization of microlites during magma ascent: the fluid mechanics of 1980–1986 eruptions at Mount St Helens. Bulletin of Volcanology, 57, 356–370.

Gualda, G.A.R., Ghiorso, M.S., Lemons, R.V., and Carley, T.L. (2012) Rhyolite-MELTS: a Modified Calibration of MELTS Optimized for Silica-rich, Fluid-bearing Magmatic Systems. Journal of Petrology, 53, 875–890.

593 Hamada, M., and Fujii, T. (2007) H2O-rich island arc low-K tholeiite magma inferred
594 from Ca-rich plagioclase-melt inclusion equilibria. Geochemical Journal, 41, 437–
595 461.

596 Hammer, J.E., and Rutherford, M.J. (2002) An experimental study of the kinetics of
597 decompression-induced crystallization in silicic melt. Journal of Geophysical
598 Research, 107.

599 Housh, T.B., and Luhr, J.F. (1991) Plagioclase-melt equilibria in hydrous systems.
600 American Mineralogist, 76, 477–492.

601 Humphreys, M., Blundy, J., and Sparks, R. (2008) Shallow-level decompression
602 crystallisation and deep magma supply at Shiveluch Volcano. Contributions to
603 Mineralogy and Petrology, 155, 45–61.

604 Humphreys, M., Edmonds, M., Christopher, T., and Hards, V. (2009a) Chlorine
605 variations in the magma of Soufriere Hills Volcano, Montserrat: Insights from Cl
606 in hornblende and melt inclusions. Geochimica et Cosmochimica Acta, 73, 5693–
607 5708.

608 Humphreys, M., Christopher, T., and Hards, V. (2009b) Microlite transfer by
609 disaggregation of mafic inclusions following magma mixing at Soufriere Hills
610 volcano, Montserrat. Contributions to Mineralogy and Petrology, 157, 609–624.

611 Humphreys, M., Edmonds, M., Christopher, T., and Hards, V. (2010) Magma
612 hybridisation and diffusive exchange recorded in heterogeneous glasses from
613 Soufriere Hills Volcano, Montserrat. Geophysical Research Letters, 37.

614 Johannes, W. (1984) Beginning of melting in the granite system Qz-Or-Ab-An-H2O.
615 Contributions to Mineralogy and Petrology, 86, 264–273.

616 Kennedy, A.., Lofgren, G.E., and Wasserburg, G.J. (1993) An experimental study of trace
617 element partitioning between olivine, orthopyroxene and melt in chondrules:
618 equilibrium values and kinetic effects. Earth and Planetary Science Letters, 115,
619 177–195.

620 Kudo, A.M., and Weill, D.F. (1970) An igneous plagioclase thermometer. Contributions
621 to Mineralogy and Petrology, 25, 52–65.

622 Lange, R.A., Frey, H.M., and Hector, J. (2009) A thermodynamic model for the
623 plagioclase-liquid hygrometer/thermometer. American Mineralogist, 94, 494–506.

624 Mann, C.P., Wallace, P.J., and Stix, J. (2013) Phenocryst-hosted melt inclusions record
625 stalling of magma during ascent in the conduit and upper magma reservoir prior to
626 vulcanian explosions, Soufriere Hills volcano, Montserrat, West Indies. Bulletin
627 of Volcanology, 75, 687.

628 Martel, C., and Schmidt, B.C. (2003) Decompression experiments as an insight into
629 ascent rates of silicic magmas. Contributions to Mineralogy and Petrology, 144,
630 397–415.

631 Milman-Barris, M.S., Beckett, J.R., Baker, M.B., Hofmann, A.E., Morgan, Z., Crowley,
632 M.R., Vielzeuf, D., and Stolper, E. (2008) Zoning of phosphorus in igneous
633 olivine. Contributions to Mineralogy and Petrology, 155, 739–765.

634 Mollo, S., Del Gaudio, P., Ventura, G., Iezzi, G., and Scarlato, P. (2010) Dependence of
635 clinopyroxene composition on cooling rate in basaltic magmas: Implications for
636 thermobarometry. Lithos, 118, 302–312.

637 Mollo, S., Putirka, K., Iezzi, G., Del Gaudio, P., and Scarlato, P. (2011) Plagioclase–melt
638 (dis)equilibrium due to cooling dynamics: Implications for thermometry,
639 barometry and hygrometry. Lithos, 125, 221–235.

640 Newcombe, M.E., Fabbrizio, A., Zhang, Y., Ma, C., Voyer, M.L., Guan, Y., Eiler, J.M.,
641 Saal, A.E., and Stolper, E.M. (2014) Chemical zonation in olivine-hosted melt
642 inclusions. Contributions to Mineralogy and Petrology, 168, 1–26.

643 Newman, S., and Lowenstern, J.B. (2002) VolatileCalc: a silicate melt–H2O-CO2
644 solution model written in Visual Basic for excel. Computers & Geosciences, 28,
645 597–604.

646 Panjasawatwong, Y., Danyushevsky, L.V., Crawford, A.J., and Harris, K.L. (1995) An
647 experimental study of the effects of melt composition on plagioclase-melt
648 equilibria at 5 and 10 kbar: implications for the origin of magmatic high-An
649 plagioclase. Contributions to Mineralogy and Petrology, 118, 420–432.

650 Pichavant, M., Costa, F., Burgisser, A., Scaillet, B., Martel, C., and Poussineau, S. (2007)
651 Equilibration Scales in Silicic to Intermediate Magmas Implications for
652 Experimental Studies. Journal of Petrology, 48, 1955–1972.

653 Putirka, K., and Condit, C.D. (2003) Cross section of a magma conduit system at the
654 margin of the Colorado Plateau. Geology, 31, 701–704.

655 Putirka, K.D. (2005) Igneous thermometers and barometers based on plagioclase + liquid
656 equilibria: Tests of some existing models and new calibrations. American
657 Mineralogist, 90, 336–346.

658 ——— (2008) Thermometers and barometers for volcanic systems. In Minerals,
659 Inclusions, and Volcanic Processes Vol. 69, pp. 61–120.

660 Ridolfi, F., Renzulli, A., and Puerini, M. (2010) Stability and chemical equilibrium of
661 amphibole in calc-alkaline magmas: an overview, new thermobarometric
662 formulations and application to subduction-related volcanoes. Contributions to
663 Mineralogy and Petrology, 160, 45–66.

664 Rutherford, M.J., and Devine, J.D. (2003) Magmatic conditions and magma ascent as
665 indicated by hornblende phase equilibria and reactions in the 1995-2002 Soufriere
666 Hills magma. Journal of Petrology, 44, 1433–1454.

667 Sisson, T.W., and Grove, T.L. (1993) Experimental investigations of the role of H2O in
668 calc-alkaline differentiation and subduction zone magmatism. Contributions to
669 Mineralogy and Petrology, 113, 143–166.

670 Waters, L.E. (2013) The effect of degassing of H2O on crystallization and oxidation in
671 highly evolved magmas: Implications for the origin of rhyolite liquids. PhD,
672 University of Michigan.

673 Waters, L.E., and Lange, R.A. (n.d.) An updated calibration of the plagioclase-liquid
674 hygrometer-thermometer applicable to basalts through rhyolites. American
675 Mineralogist (in press).

676 Welsch, B., Hammer, J., and Hellebrand, E. (2014) Phosphorus zoning reveals dendritic
677 architecture of olivine. Geology, 42, 867–870.

678

679

680 Figure 1

681 Equilibrium relationships between rhyolitic melt H_2O,temperature and plagioclase
682 XAn, calculated using Putirka (2005) and Lange et al. (2009). (a) Contours of
683 constant plagioclase composition in H_2O-T space. Large grey diamonds are
684 interpolated from the phase diagram of Couch et al. (2003). (b) Contours of constant
685 temperature in H_2O-X_{An} space. Also shown is RhyoliteMELTS modelling of
686 isothermal decompression for rhyolitic melt (bold lines, 825-875 °C) and basaltic
687 andesite melt (thin black lines, 1000-1100 °C).

688

689 Figure 2

690 Contours of constant pressure (assuming H_2O saturation, i.e. P_{tot} = pH_2O) in T–X_{An}
691 space, calculated for rhyolitic melt using Putirka (2005) and Lange et al. (2009).
692 Large circles are interpolated from the phase diagram of Couch et al. (2003) for 160
693 MPa (black) and 200 MPa (grey). Also shown is RhyoliteMELTS modelling of
694 isobaric cooling in rhyolitic melt (25-200 MPa).

695

696 Figure 3

697 Theoretical variation of plagioclase-liquid K_D for rhyolitic melt (as defined by
698 Putirka 2005; 2008) with calculated temperature (T_{calc}) as a function of pressure
699 (assuming H_2O saturation, i.e. P_{tot} = pH_2O) (a), and with pH_2O as a function of
700 temperature (b). Points in (a) represent increments of 10 mol% X_{An}.

701

702 Figure 4

703 H_2O concentration in experimentally decompressed glasses from Martel & Schmidt
704 (2003), Brugger & Hammer (2010) and Cichy et al. (2011), in comparison with
705 isobaric (solubility) data from Mangan & Sisson (2000). Also shown is rhyolite
706 solubility curve from VolatileCalc (Newman & Lowenstern 2002). All data have H_2O
707 concentrations in excess of the solubility limit for the experimental quench
708 pressure, indicating kinetically inhibited degassing.
709
710 Figure 5
711 Variation of calculated temperature (T_{calc}, using model A from Putirka, 2005) and K_D
712 with pH_2O in experimentally decompressed glasses from Brugger & Hammer (2010;
713 a, b), Cichy et al. (2011; c, d) and Martel & Schmidt (2003; e, f). Grey bar with black
714 line shows the experimental run temperature in each case ± 5 °C.
715
716 Figure 6
717 Variation of calculated temperature (T_{calc}, using model A from Putirka, 2005) and K_D
718 with decompression rate in experimentally decompressed glasses from Brugger &
719 Hammer (2010; a, b), Cichy et al. (2011; c, d) and Martel & Schmidt (2003; e, f). Grey
720 bar with black line shows the experimental run temperature in each case ± 5 °C.
721
722 Figure 7
723 (a) Variation of calculated temperature (T_{calc}, using model A from Putirka, 2005)
724 with H_2O concentration of plagioclase-hosted melt inclusions from Soufrière Hills,
725 Montserrat (Humphreys et al. 2009); Mt Unzen, Japan (Botcharnikov et al. 2007);

Mount St Helens, USA (Blundy et al. 2006); Shiveluch, Kamchatka (Blundy et al. 2006) and Izu Oshima (Hamada & Fujii 2007). Constant-X_{An} contours are shown for comparison (symbols as figure 1). (b) Variations of T_{calc} with X_{An} of the host plagioclase phenocryst for the same melt inclusion suites. Constant-pH_2O contours are shown for comparison (symbols as figure 2).

Figure 8

Variation of K_D with (a) plagioclase X_{An} and (b) glass H_2O concentration for melt inclusion datasets from the literature. Dark circles – Mount St Helens (Blundy et al. 2006); grey squares – Shiveluch (Blundy et al. 2006); dashes – Soufrière Hills, Montserrat (Humphreys et al. 2009); crosses - Izu Oshima (Hamada & Fujii 2007); dark triangles - Mt Unzen (Botcharnikov et al. 2007).

Figure 9

Regression of T_{calc} with each of the parameters that make up the calculation, (a) Ca_L, (b) Na_L, (c) Al_L, (d) Si_L, (e) H_2O and (f) X_{An}. Dark circles – Mount St Helens, grey squares – Shiveluch (Blundy et al. 2006). Linear regression trends and equations are given for any significant regressions ($R^2 \geq 0.15$), with Mount St Helens regressions in black and Shiveluch in grey. The most significant parameter controlling T_{calc} is the H_2O content of the glass.

Figure 10

748 Regression of T_{calc} with each of the parameters that make up the calculation, (a) Ca_L,
749 (b) Na_L, (c) Al_L, (d) Si_L, (e) H_2O and (f) X_{An}. Dashes – Soufriere Hills, Montserrat
750 (Humphreys et al. 2009); crosses - Izu Oshima (Hamada & Fujii 2007); dark
751 triangles - Mt Unzen (Botcharnikov et al. 2008). Linear regression trends and
752 equations are given for any significant regressions ($R^2 \geq 0.15$) in each dataset. The
753 most significant parameter controlling T_{calc} is the H_2O content of the glass.
754
755 Figure 11
756 Back-scattered SEM image illustrating the complexity of plagioclase zoning that is
757 common in intermediate calc-alkaline lavas. Melt inclusions are dark blebs (some
758 annotated 'MI'). White dashed lines outline clear resorptive zoning 'events' that
759 leave irregular boundaries and may entrap melt inclusions.
760

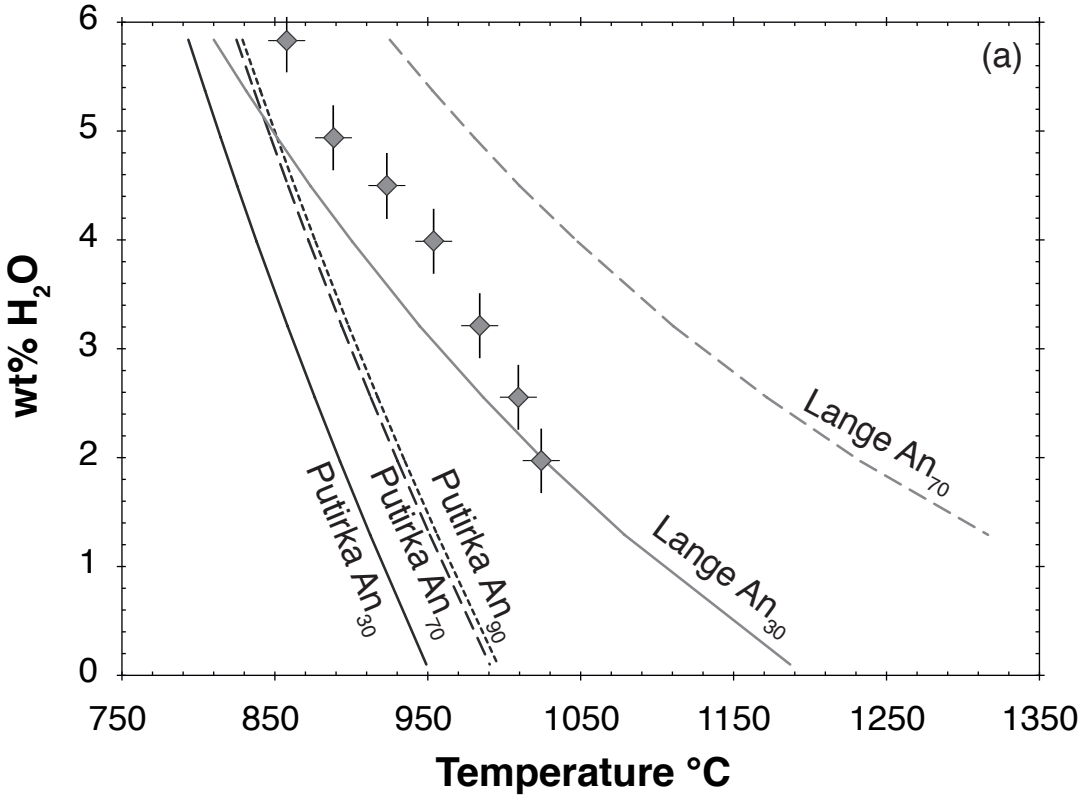
(a)
wt% H_2O
Temperature °C
Putirka An_{30}
Putirka An_{70}
Putirka An_{90}
Lange An_{70}
Lange An_{30}

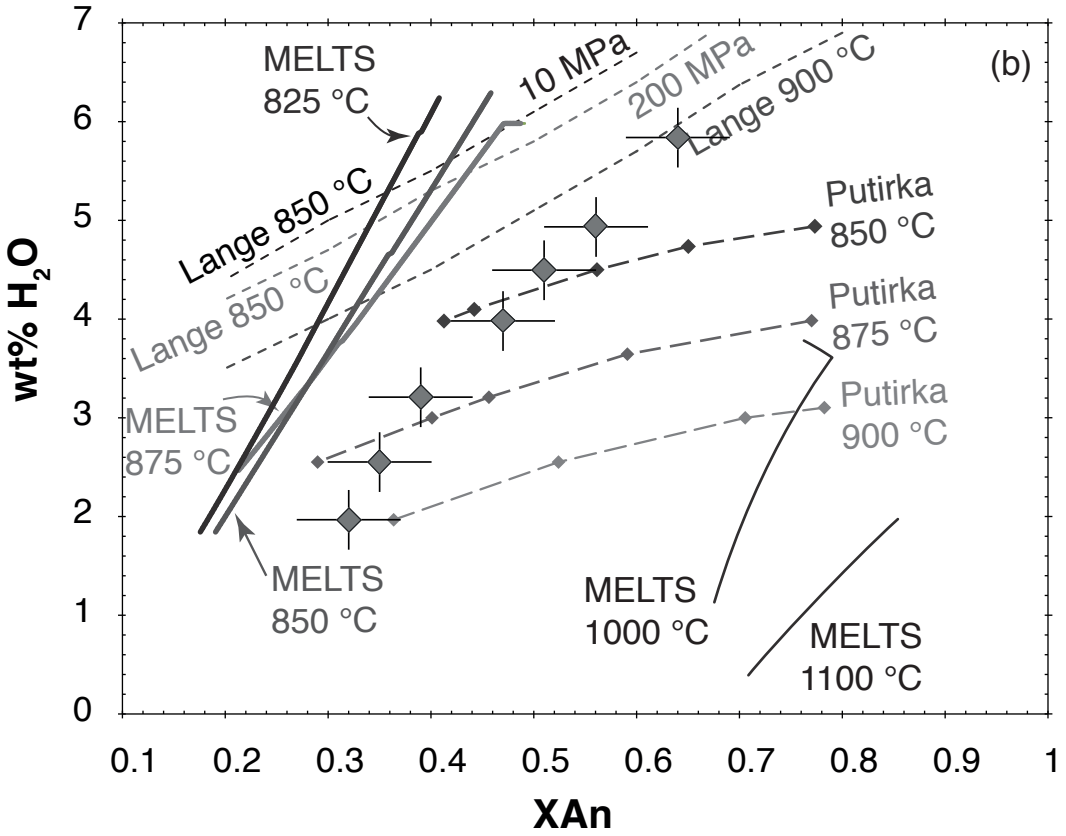
(b)
wt% H_2O
XAn
MELTS 825 °C
10 MPa
200 MPa
Lange 900 °C
Lange 850 °C
Lange 850 °C
Putirka 850 °C
Putirka 875 °C
Putirka 900 °C
MELTS 875 °C
MELTS 850 °C
MELTS 1000 °C
MELTS 1100 °C

Figure 1

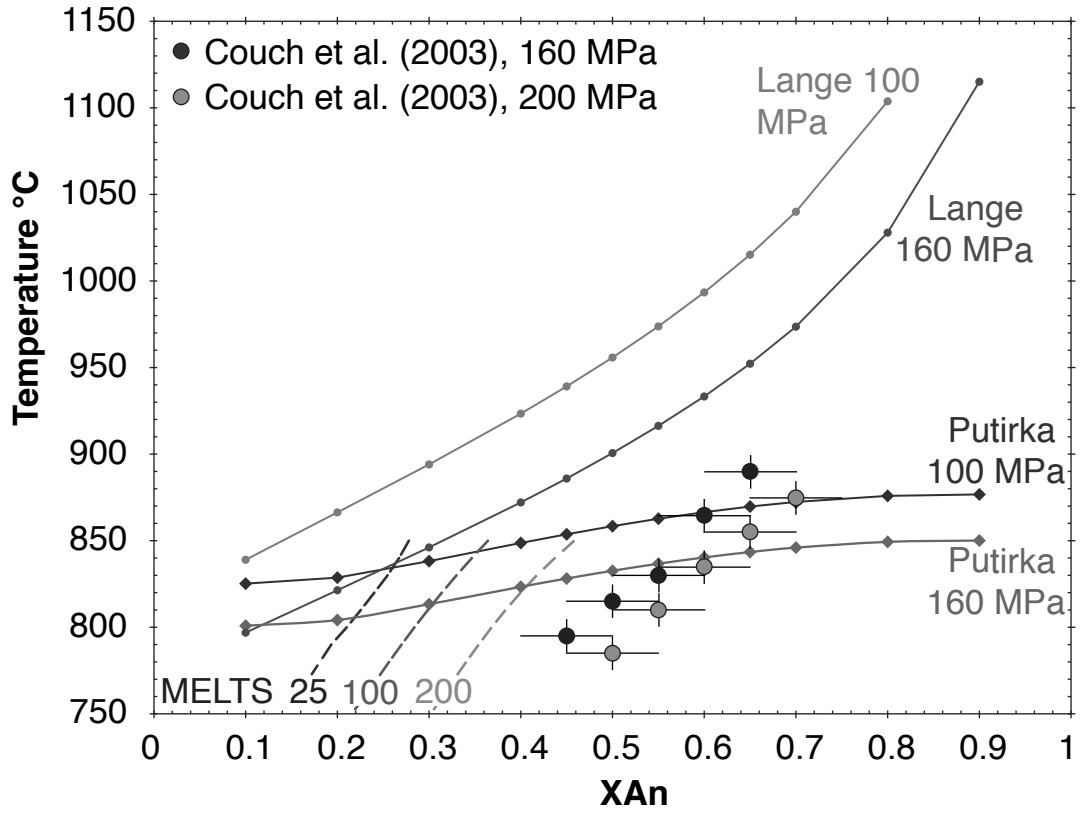
Couch et al. (2003), 160 MPa
Couch et al. (2003), 200 MPa
Lange 100 MPa
Lange 160 MPa
Putirka 100 MPa
Putirka 160 MPa
MELTS 25 100 200
Temperature °C
XAn
1150
1100
1050
1000
950
900
850
800
750
0
0.1
0.2
0.3
0.4
0.5
0.6
0.7
0.8
0.9
1

Figure 2

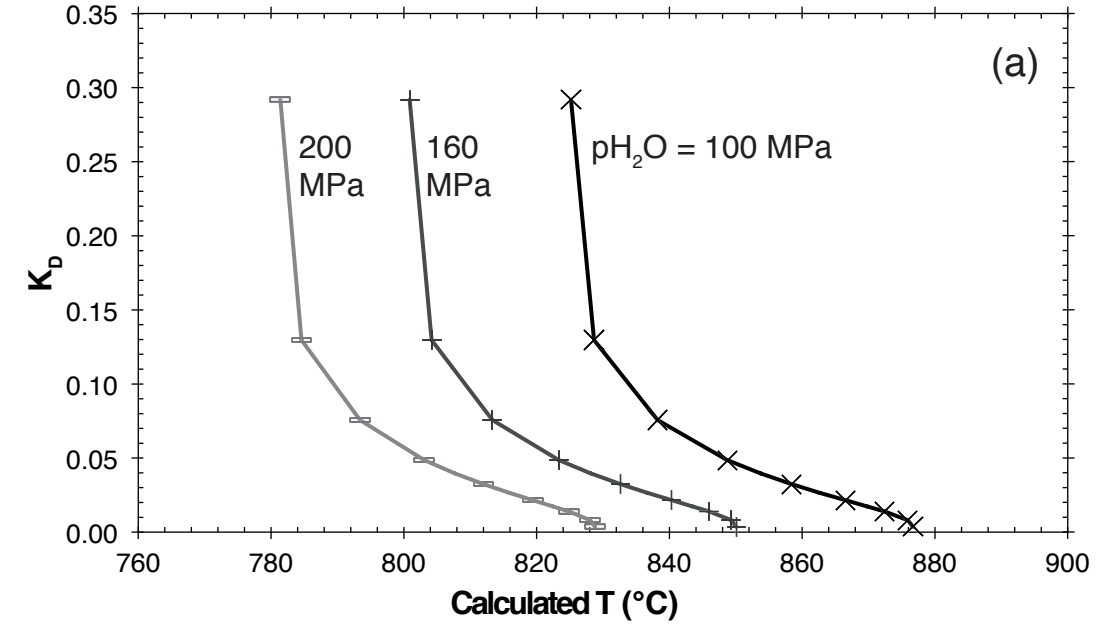
(a)
200 MPa
160 MPa
pH2O = 100 MPa
KD
Calculated T (°C)

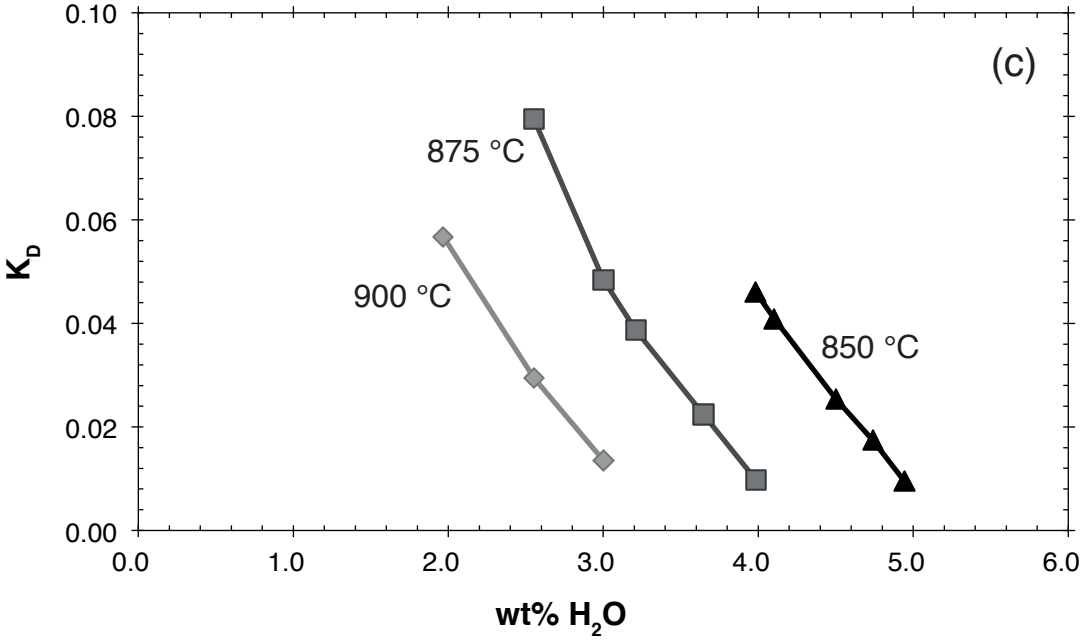
(c)
875 °C
900 °C
850 °C
KD
wt% H2O

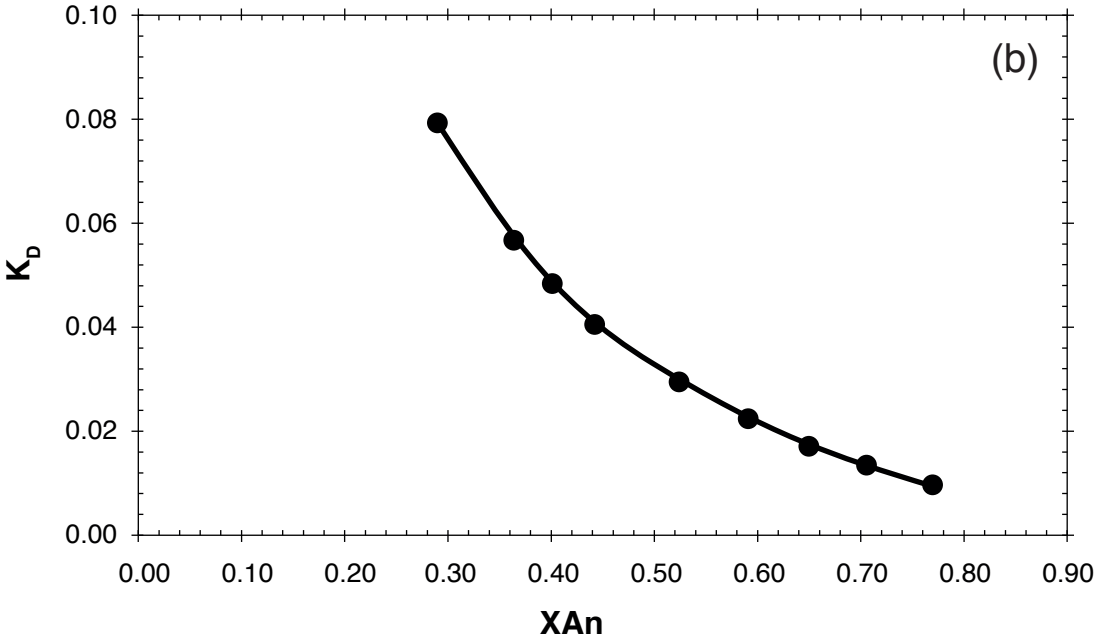
(b)
KD
XAn

Figure 3

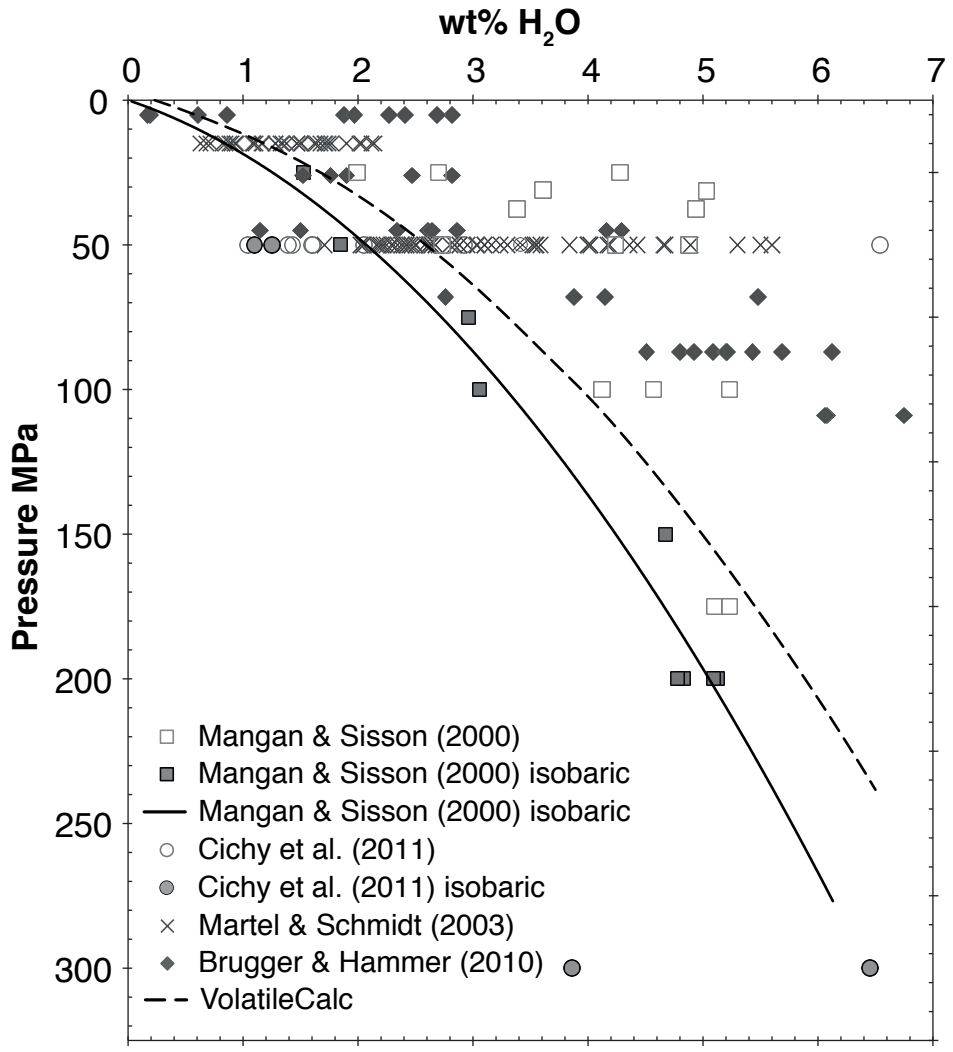
wt% H2O
0
1
2
3
4
5
6
7
Pressure MPa
0
50
100
150
200
250
300
Mangan & Sisson (2000)
Mangan & Sisson (2000) isobaric
Mangan & Sisson (2000) isobaric
Cichy et al. (2011)
Cichy et al. (2011) isobaric
Martel & Schmidt (2003)
Brugger & Hammer (2010)
VolatileCalc

Figure 4

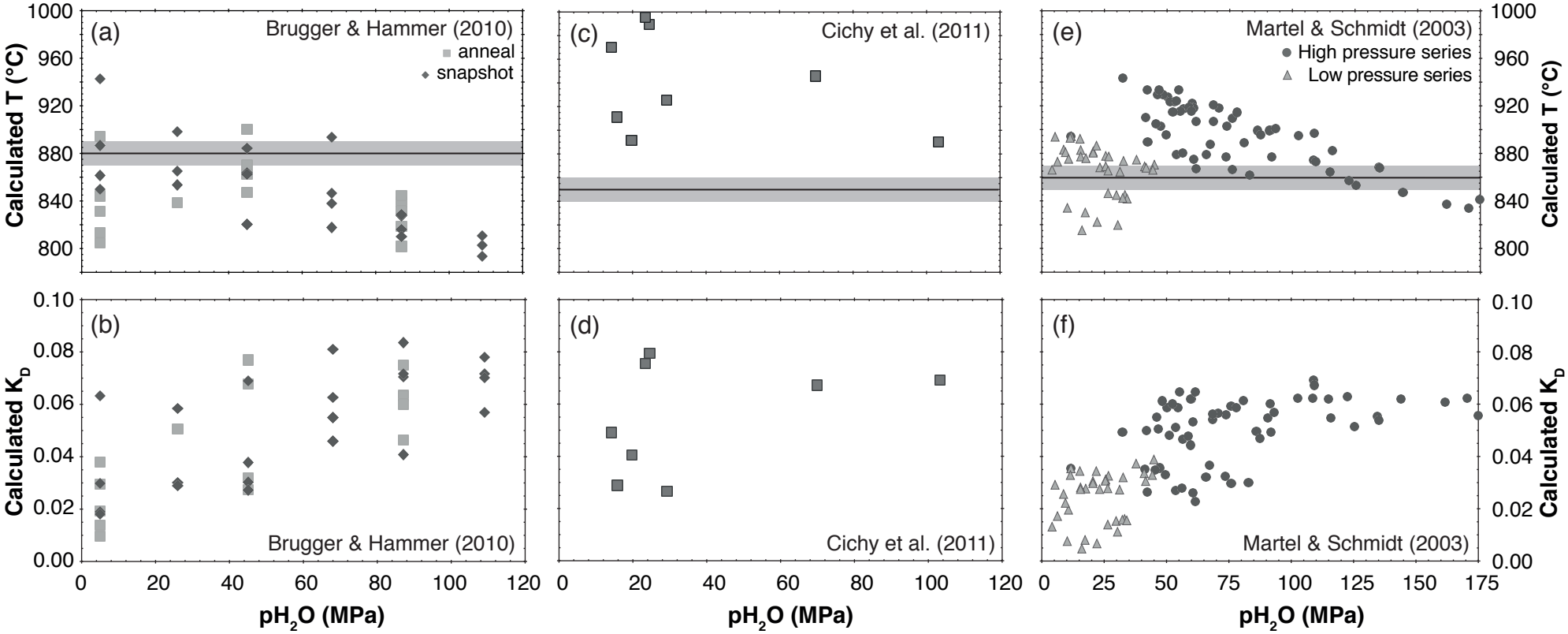
(a)
Brugger & Hammer (2010)
anneal
snapshot
(c)
Cichy et al. (2011)
(e)
Martel & Schmidt (2003)
High pressure series
Low pressure series
Calculated T (°C)
1000
960
920
880
840
800
(b)
(d)
(f)
Calculated K_D
0.10
0.08
0.06
0.04
0.02
0.00
0
20
40
60
80
100
120
0
25
50
75
100
125
150
175
pH_2O (MPa)

Figure 5

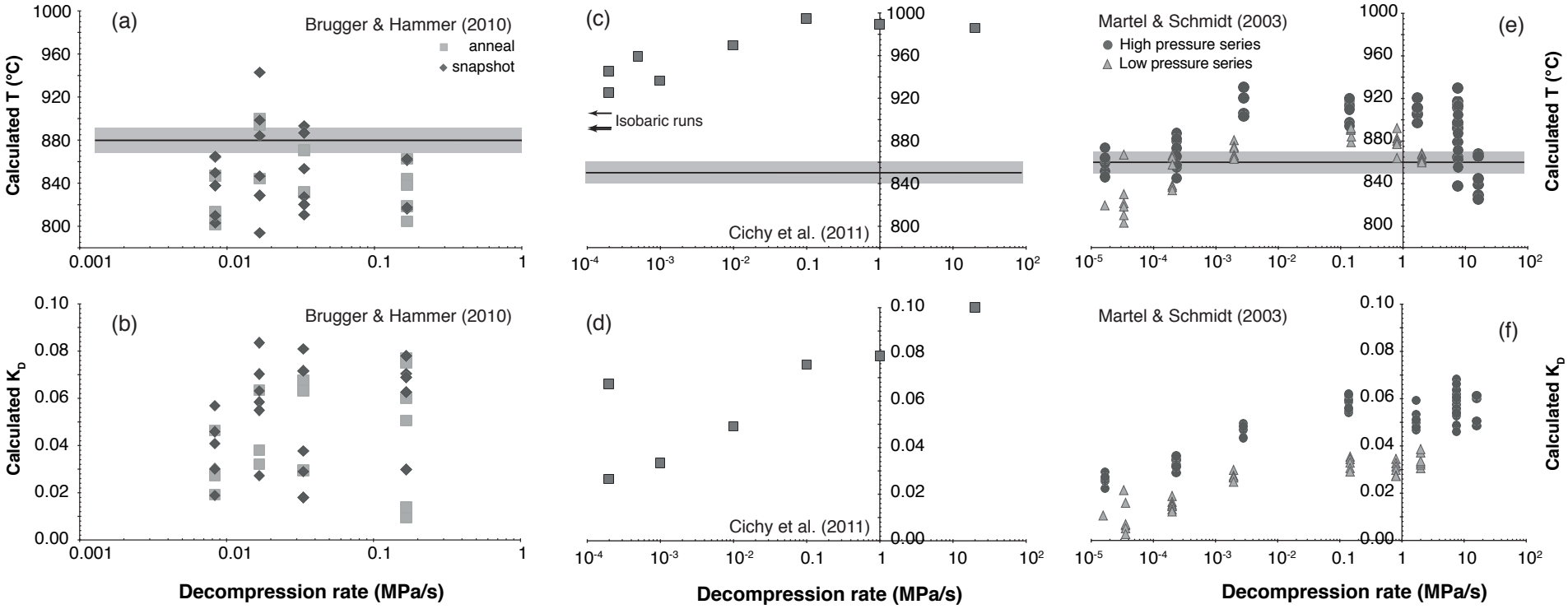
(a)
Brugger & Hammer (2010)
anneal
snapshot
Calculated T (°C)
(b)
Brugger & Hammer (2010)
Calculated K_D
Decompression rate (MPa/s)
(c)
Isobaric runs
Cichy et al. (2011)
(d)
Cichy et al. (2011)
Decompression rate (MPa/s)
Martel & Schmidt (2003)
High pressure series
Low pressure series
(e)
Calculated T (°C)
Martel & Schmidt (2003)
(f)
Calculated K_D
Decompression rate (MPa/s)

Figure 6

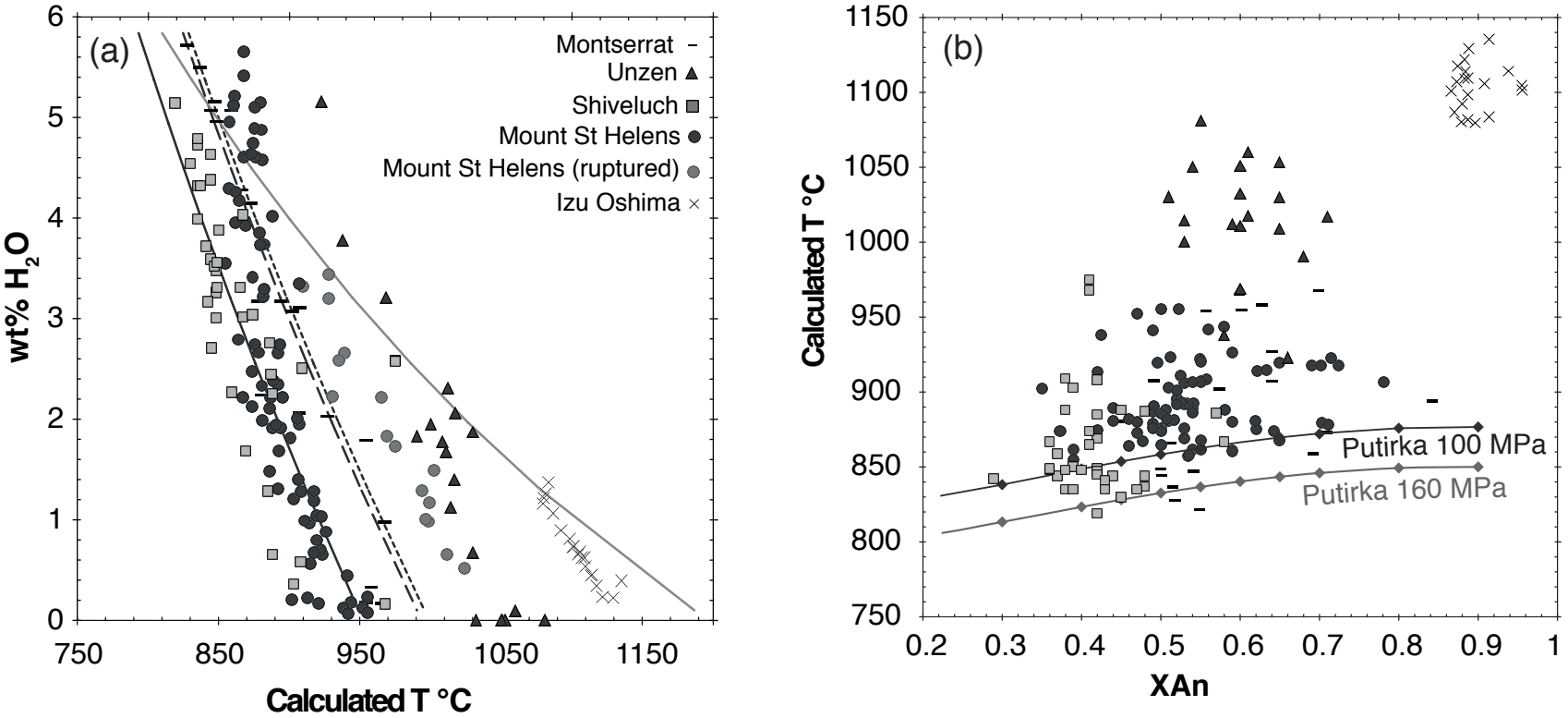
(a)
Montserrat
Unzen
Shiveluch
Mount St Helens
Mount St Helens (ruptured)
Izu Oshima
wt% H2O
Calculated T °C
(b)
Calculated T °C
XAn
Putirka 100 MPa
Putirka 160 MPa

Figure 7

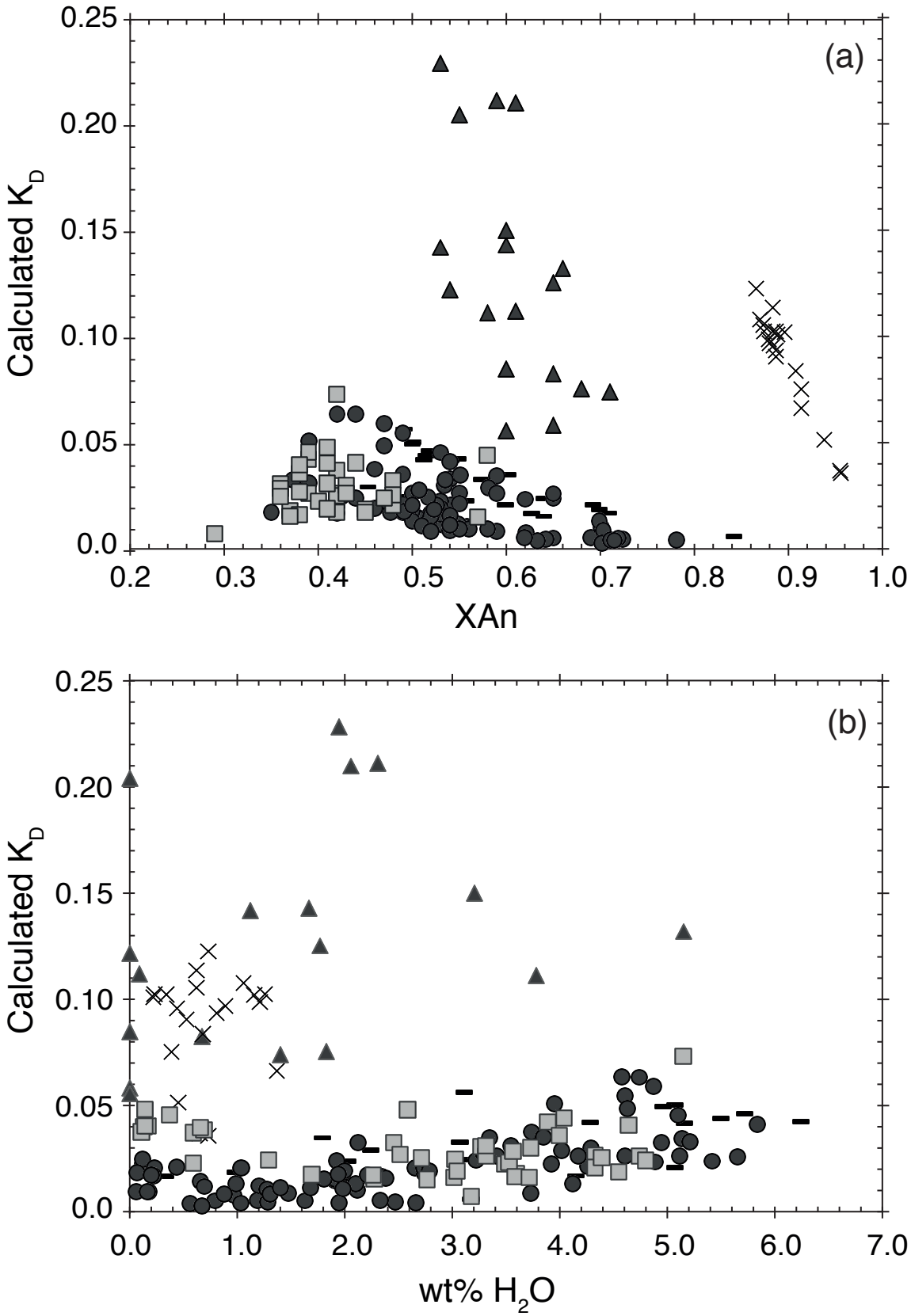
(a)
Calculated K_D
0.25
0.20
0.15
0.10
0.05
0.0
0.2
0.3
0.4
0.5
0.6
0.7
0.8
0.9
1.0
XAn
(b)
Calculated K_D
0.25
0.20
0.15
0.10
0.05
0.0
0.0
1.0
2.0
3.0
4.0
5.0
6.0
7.0
wt% H_2O

Figure 8

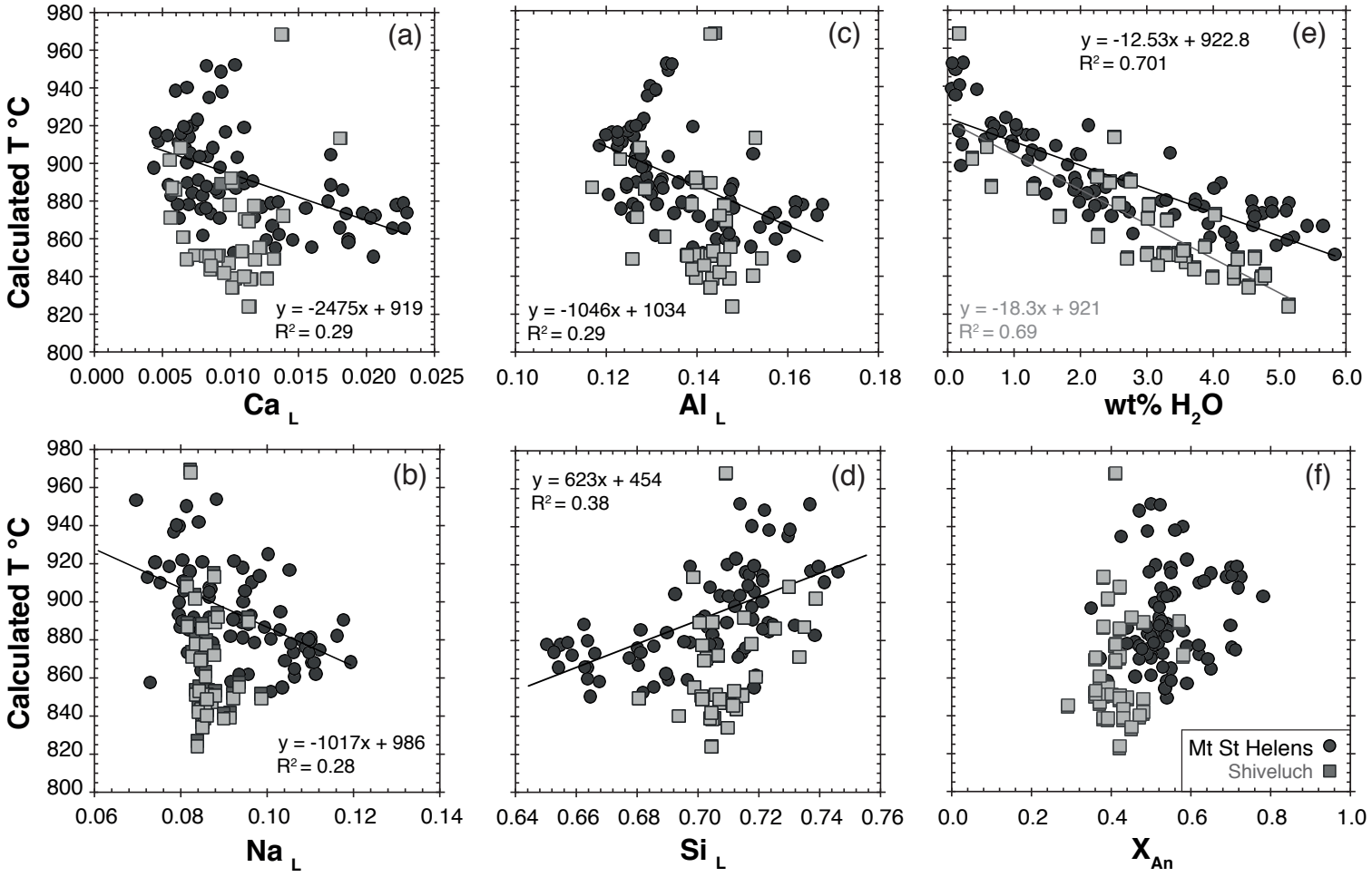
(a)
y = -2475x + 919
R² = 0.29
Ca L
(c)
y = -1046x + 1034
R² = 0.29
Al L
(e)
y = -12.53x + 922.8
R² = 0.701
y = -18.3x + 921
R² = 0.69
wt% H2O
(b)
y = -1017x + 986
R² = 0.28
Na L
(d)
y = 623x + 454
R² = 0.38
Si L
(f)
Mt St Helens
Shiveluch
X An
Calculated T °C

Figure 9

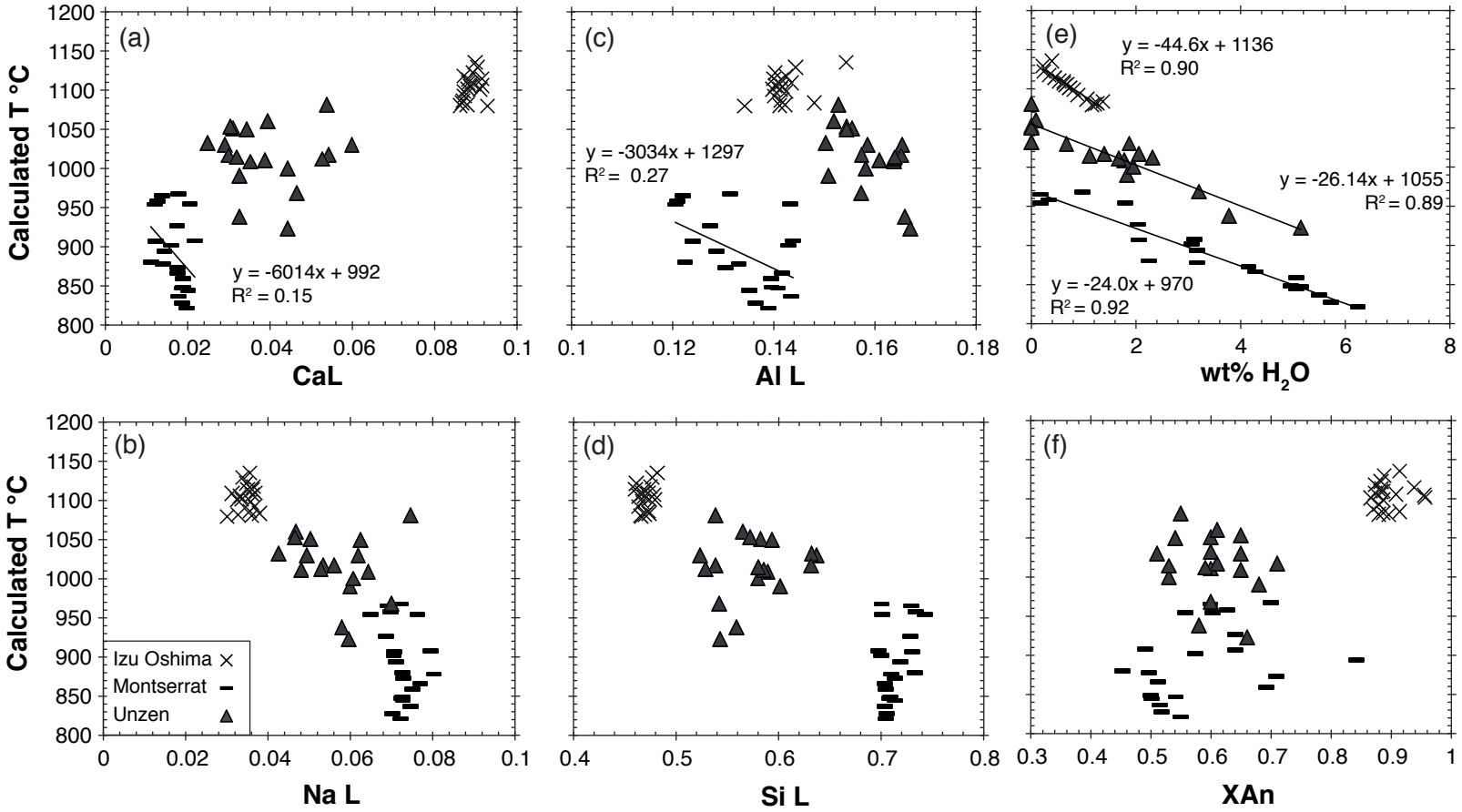
(a)
y = -6014x + 992
R² = 0.15
Calculated T °C
CaL
(c)
y = -3034x + 1297
R² = 0.27
Al L
(e)
y = -44.6x + 1136
R² = 0.90
y = -26.14x + 1055
R² = 0.89
y = -24.0x + 970
R² = 0.92
wt% H2O
(b)
Izu Oshima
Montserrat
Unzen
Na L
(d)
Si L
(f)
XAn

Figure 10

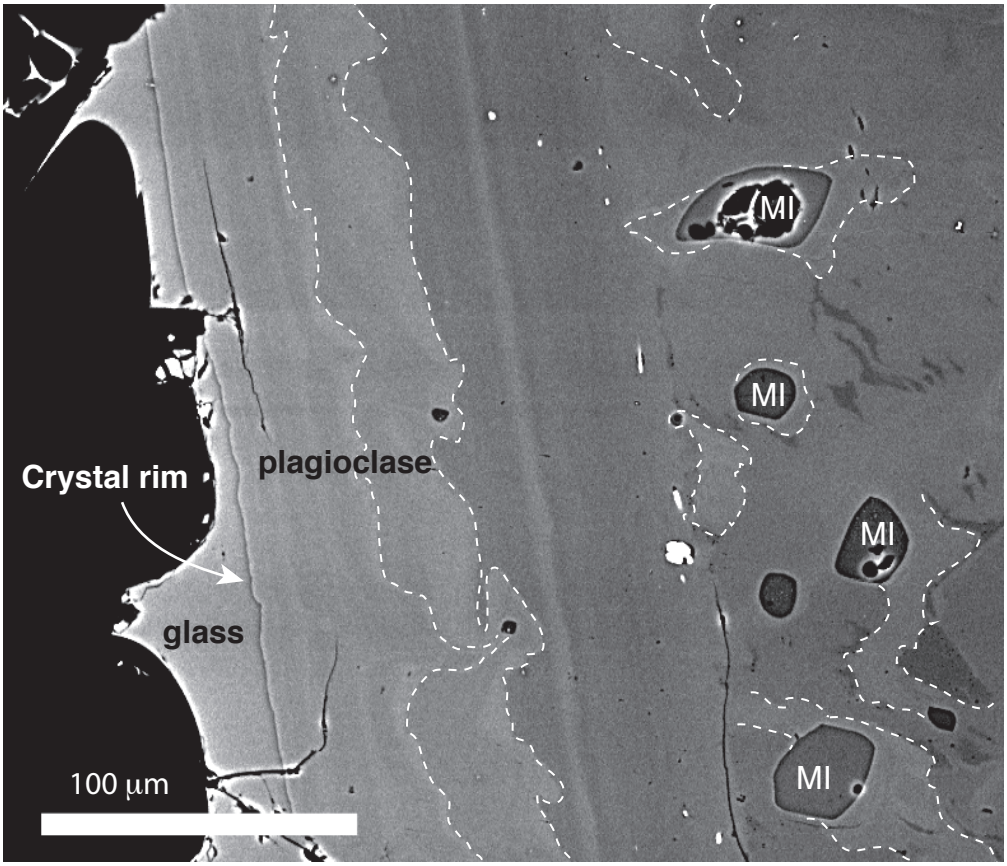

Figure 11

	MVO1524b_112	ol101mi1
SiO_2	73.32	52.20
TiO_2	0.26	0.86
Al_2O_3	11.66	15.80
FeO_T	1.56	12.40
MgO	0.28	5.72
MnO	0.07	0.22
CaO	1.34	10.34
Na_2O	4.28	1.82
K_2O	2.54	0.31
Cl	0.26	0.04
H_2O	3.16	1.24
Total	98.73	100.95

Table 1.
Composition of rhyolite melt inclusion (MVO1524b_112, from Humphreys et al. 2009) and basaltic andesite melt (ol101mi1, from Hamada & Fujii 2007) used for MELTS modelling and calculations shown in figures 1-4.